https://doi.org/10.5194/wes-2019-107
Preprint. Discussion started: 10 January 2020

eawe european academy of wind energy
Open Access WIND ENERGY SCIENCE DISCUSSIONS

Characterization of a new perturbation system for gust generation: The Chopper

Ingrid Neunaber[1] and Caroline Braud[1]
[1]LHEEA - Ecole Centrale Nantes, CNRS, 1 Rue de la Noë, 44321 Nantes, France
Correspondence: Ingrid Neunaber (ingrid.neunaber@ec-nantes.fr)

Abstract. We present a new system for the generation of rapid, strong flow disturbances in a wind tunnel that was recently installed at Ecole Centrale Nantes. The system is called *the chopper*, and it consists of a rotating bar cutting through the inlet of a wind tunnel test section, thus generating a gust that travels downstream. The flow generated by the chopper is investigated with respect to the rotational frequency using an array equipped with hot-wires that is traversed downstream the flow field. It is found that the gust can be described as a superposition of the mean gust velocity, an underlying gust shape and additional turbulence. Following this approach, the evolution of the mean gust velocity and turbulence intensity are presented, and the evolution of the underlying gust shape is explained. The turbulence is shown to be characterized by an integral length scale of approximately half the chopper blade width and a turbulence decay according to $E(f) \propto f^{-5/3}$.

1 Introduction

Wind energy converters are operating in the atmospheric boundary layer that is naturally turbulent. One consequence of the turbulence within the atmospheric boundary layer is that the wind turbine experiences higher loads (see e.g. Frandsen (2007) and Lee et al. (2012)). To still ensure the durability and safety of a wind turbine during its planned lifetime of generally 20 years, the IEC 61400-1 norm gives a set of design requirements (cf. IEC-61400-1-4 (2019)). These requirements depend on the site specifications: Based on the reference wind speed and the turbulence characteristics obtained from site assessment, wind turbines are assigned to a class. This class determines the wind conditions a turbine within the class has to withstand. The wind conditions used for load and safety calculations are separated into normal wind conditions and different extreme wind conditions. One of the extreme wind conditions is the extreme operating gust (EOG), an artificial gust that is assumed to occur once every 50 years. The gust is modeled as Mexican hat wavelet and characterized by a duration $\Delta t = 10.5\,\mathrm{s}$ and a velocity amplitude Δu that depends on the velocity u at hub height z_{hub}, the rotor diameter D and the turbine class. Examples of an EOG calculated for different hub height velocities for a wind turbine of class I.A with diameter $D = 136\,\mathrm{m}$ and hub height $z_{hub} = 155\,\mathrm{m}$ can be found in figure 1. At $u = 25\,\mathrm{m/s}$, the velocity increases by $\Delta u = 9.8\,\mathrm{m/s}$ within $2.8\,\mathrm{s}$. Such a rapid change can not be accounted for with today's control mechanisms and therefore, the aerodynamics at the rotor blade are strongly affected. The interactions between the three-dimensional, turbulent inflow and the rotor blades are highly complex and not well understood. One option to gain knowledge of the aerodynamic effects that strong gusts like the EOG induce to a turbine in operation are wind tunnel experiments on airfoils. However, the reproduction of strong gusts in a wind tunnel can be

https://doi.org/10.5194/wes-2019-107
Preprint. Discussion started: 10 January 2020

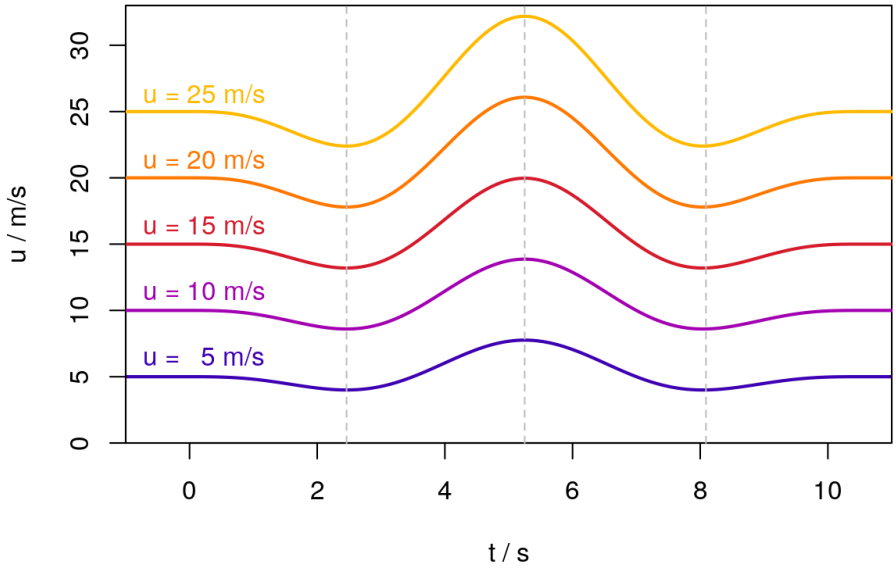

Figure 1. Examples of the extreme operating gust according to the IEC-61400-1 norm calculated for different hub height velocities for a wind turbine of class I.A with diameter $D = 136\,\text{m}$, hub height $z_{hub} = 155\,\text{m}$ like the Enercon E-136.

challenging. Moreover, the extend to which turbulence should be added to the gust is a supplementary parameter to tune since experiments with turbulence are more realistic on the one side, but complicate the isolation of single effects on the change of aerodynamics on the blade on the other side. Often, experiments are designed to investigate one isolated effect, and there are different approaches to create gusts in the wind tunnel.

One approach is the generation of periodic gusts in the wind tunnel. This can for example be done by using a single pitching and plunging airfoil, as Wei et al. (2019a) demonstrate, who aim for a low-turbulent, lateral, periodic gust. In Wei et al. (2019b), the authors reproduce a sinusoidal gust in lateral and longitudinal direction using an array of oscillating 2D airfoils at the inlet of the wind tunnel. The same setup is used in Wester et al. (2018) to generate a lateral gust similar to the artificial EOG proposed in the IEC61400-1 norm. In a different approach, Tang et al. (1996) use rotating slotted cylinders to generate periodic gusts in the lateral and longitudinal directions, and they are able to create sinusoidal velocity fluctuations with an amplitude of $\Delta u = 5\,\text{m/s}$ at an inflow velocity of $u = 23\,\text{m/s}$. While the velocity amplitude is only half of the presented EOG's velocity amplitude at $u = 25\,\text{m/s}$, one advantage of this system is the simple, low-cost design. Another device that is capable of creating customized flows and also gusts is an active grid. The most common design was proposed by Hideharu (1991), the so-called 'Makita-style' active grid. The initial design has been modified by different groups to over the past years. In Petrović et al. (2019) and Traphan et al. (2018), it was demonstrated that Makita-style active grids can be used to generate gusts matching the one proposed as EOG in IEC-61400-1-4 (2019). While the flexibility and the stage of research are two major advantages of the Makita-style active grid, disadvantages include high complexity, high cost and maintenance.

https://doi.org/10.5194/wes-2019-107
Preprint. Discussion started: 10 January 2020

eawe european academy of wind energy
Open Access WIND ENERGY SCIENCE DISCUSSIONS

With the exception of Traphan et al. (2018) and Petrović et al. (2019), all the above-presented experiments focus on the generation of specific gusts tailored to investigate isolated aerodynamic responses. Nevertheless, to understand the interaction between turbulent flow structures and the aerodynamics of a rotor blade, it is important to include turbulence when investigating the influence of EOGs. Therefore, in this study, a simple and inexpensive system for aerodynamic experiments is presented that is capable of generating large velocity fluctuations on different time scales while also inducing strong turbulence to investigate the coupled effect of a gust with turbulence on aerodynamic changes.

2 Experimental setup

In the following, the chopper and the experimental setup used to characterize the flow disturbance generated by the chopper are introduced. In figure 2, a sketch of the chopper and its installation in the closed-loop wind tunnel can be found. The chopper consists of a rectangular bar, the *chopper blade*, that rotates around its central axis which is aligned parallel to the test section. Therefore, within one revolution, the two arms of the chopper blade cross the inlet of the test section. The chopper frequency f_{CH} is defined as the frequency with which the blade arms cross the inlet, making it twice the rotational frequency, $f_{rot} = 1/2 \cdot f_{CH}$. When the blade's arms cut through the inlet of the wind tunnel, a gust is created and transported downstream the test section. The blade has a radius of $R_{CH} = 900\,\text{mm}$, a width of $w_{CH} = 200\,\text{mm}$, and a thickness of $d_{CH} = 50\,\text{mm}$. The test section's dimensions are $(500 \times 500)\,\text{mm}^2$ with a closed test section of 2300 mm length. In the following, the downstream positions will be given with respect to the chopper blade and the vertical and lateral positions with respect to the centerline of the test section. The coordinates will be normalized to the blade width. The blockage induced by the chopper varies with the angle α between the blade and the horizontal centerline of the inlet and can reach up to 40.6%. An induction sensor gives a signal every time one of the blade arms passes the horizontal centerline of the inlet ($\alpha = 0$). From this measurement, the blockage (i.e. area of chopper blade inside the cross test section versus the total area of the test section) is computed. In the following, the root of the blade corresponds to the part of the blade close to the rotation axis, while the tip of the blade corresponds to the part of the blade the furthest from the rotation axis (see figure 2).

To characterize the chopper, an array equipped with five 1D hot-wire probes of type 55P11 with a sensor length of 1.25 mm from Dantec Dynamics was used. A sketch of the probe arrangement can be found in figure 2. Four of the sensors were operated by MiniCTA modules of type 54T30 from Dantec Dynamics with a temporal resolution of 10 kHz while one sensor, the sensor positioned at the centerline, was operated using a Disa Type 55M01 Main Unit and Standard Bridge with a temporal resolution of 38 kHz as determined with a square-wave test. A temperature probe was used to monitor the temperature during calibration and measurement, and a temperature correction according to Hultmark and Smits (2010) was applied when processing the data. The hot-wires were calibrated in the range $0\,\text{m/s} \leq u \leq 55\,\text{m/s}$ using a Disa calibrator of type 55D45 with a nozzle of $60\,\text{mm}^2$. The data was collected by a D.T.MUX Recorder with a sampling frequency of $f_s = 100\,\text{kHz}$, and the data was filtered with a built-in low-pass hard-ware filter at $f_f = 40\,\text{kHz}$.

Horizontal velocity profiles were measured at nine downstream positions at the test section's centerline, and in addition, one plane perpendicular to the flow at $X = 8.675\,w_{CH}$ was scrutinized. The measurement planes are indicated in figure 2. The

https://doi.org/10.5194/wes-2019-107
Preprint. Discussion started: 10 January 2020

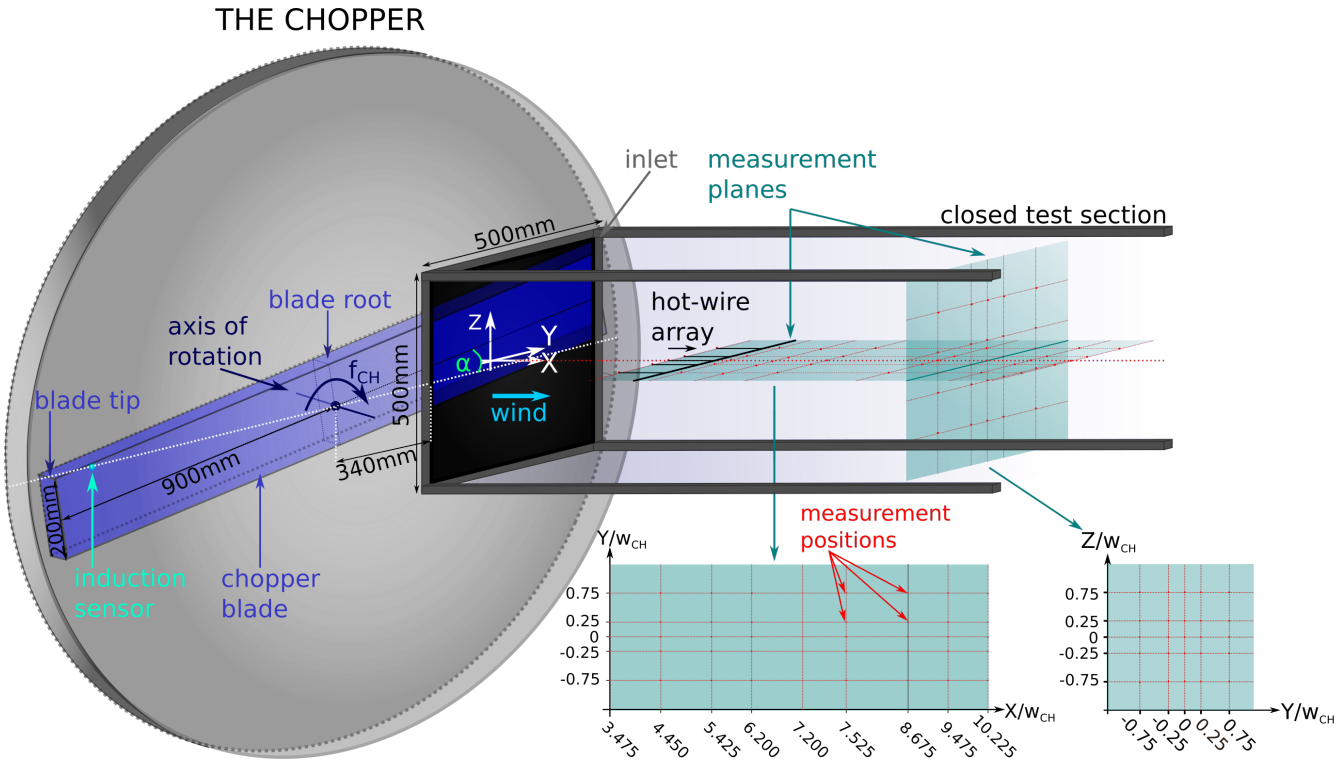

Figure 2. Experimental setup: The rotating chopper blade (blue) cuts through the inlet of the wind tunnel test section, thus generating a flow disturbance. An induction sensor returns a signal when the chopper blade crosses the horizontal centerline of the test section inlet. Measurements were carried out using an array of five hot-wire probes downstream at the positions marked with red dots within the turquoise measurement planes.

inflow velocity was $u_0 = 25\,\mathrm{m/s}$, and two chopper frequencies, $f_{CH1} = 0.04\,\mathrm{Hz}$ and $f_{CH2} = 0.4\,\mathrm{Hz}$, have been investigated. To measure a sufficient amount of gust events for each chopper frequency, the measurement times were adapted. With $t_1 = 600\,\mathrm{s}$ for $f_{CH1} = 0.04\,\mathrm{Hz}$ and $t_2 = 120\,\mathrm{s}$ for $f_{CH2} = 0.4\,\mathrm{Hz}$, respectively, more than 20 gust events were captured in each measurement.

In the next section, the results from these measurements are presented.

3 Results

In the following, the structure and the downstream evolution of the gust generated by the chopper will be presented. For a first overview, an example of the the time series will be shown in combination with the energy spectral density. The separate elements of the gust structure will be explained. Afterwards, the evolution of the gust will be investigated by looking at the average gust flow field, the gust shape and the turbulence within the gust. The analysis will include mean velocities u, turbulence

https://doi.org/10.5194/wes-2019-107
Preprint. Discussion started: 10 January 2020

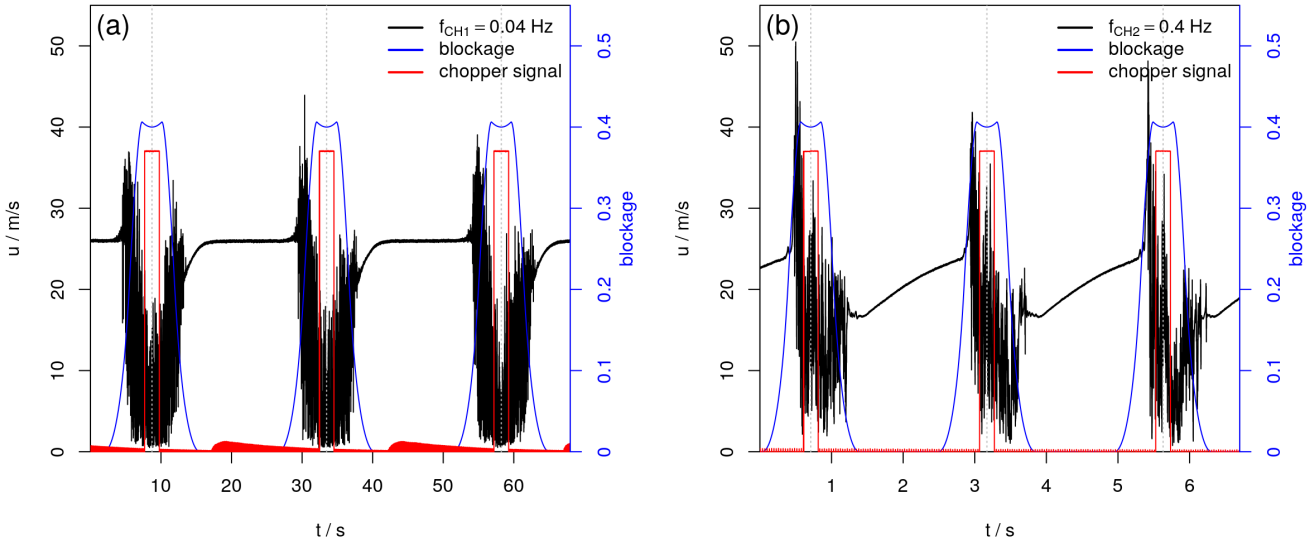

Figure 3. Gust produced by chopper, measured at the centerline $5.425 w_{CH}$ from the chopper blade: (a) $f_{CH1} = 0.04$Hz, (b) $f_{CH2} = 0.4$Hz. The blue curve indicates the blockage, the red curve the signal from the induction sensor, and the gray dashed lines the moment when the chopper blade is horizontally aligned with the inlet.

intensities TI and a spectral analysis including the computation of the integral length scale L.

3.1 Analysis of the time series

In figure 3, a part of the time series (black) that includes three gusts is plotted for both chopper frequencies. In addition, the blockage induced by the chopper (blue) and the signal from the induction sensor (red) are plotted. The measurements were carried out at the centerline in $5.425\, w_{CH}$ distance from the chopper blade. Looking at figure 3(a) ($f_{CH1} = 0.04$ Hz), it can be seen that the velocity first increases when the chopper blade enters the inlet. The velocity decreases then drastically and fast when the blockage of the inlet due to the chopper blade increases, and it recovers when the chopper blade leaves the inlet. Between the gusts, the velocity equals the inflow velocity and has a turbulence intensity of 0.3%. While the gusts evolve similarly, differences in the turbulent fluctuations are present. In case of the f_{CH2}, see figure 3(b), the result looks similarly with the difference that the velocity can not recover between the gusts. Instead it increases until the chopper blade enters the inlet anew to create the next gust. In addition, the fluctuations induced by the chopper are stronger in case of the high rotation frequency and can reach values above 50 m/s which is twice the inflow velocity.Figure 4 shows the energy spectral density $E(f)$ over frequency f of the two above presented time series measured at the centerline $5.425\, w_{CH}$ downstream the chopper blade. At low frequencies, the spectrum is flat but superimposed with the peak of the chopper frequency and its harmonics. From $f \approx 10$Hz, the energy spectral density decays with increasing frequency according to the well known $E(f) \propto f^{-5/3}$ law

https://doi.org/10.5194/wes-2019-107
Preprint. Discussion started: 10 January 2020

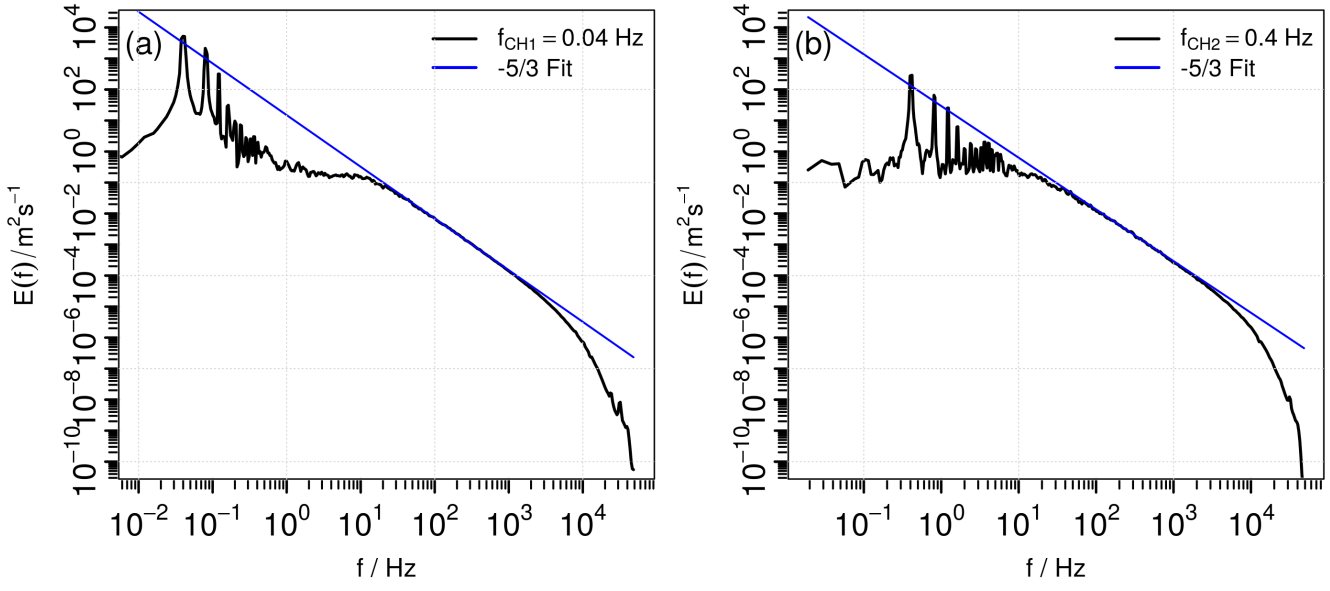

Figure 4. Energy spectral density of the measured time series at the centerline at $5.425\,w_{CH}$ distance from the inlet for the chopper frequencies (a) $f_{CH1} = 0.04\,\text{Hz}$ and (b) $f_{CH2} = 0.4\,\text{Hz}$. The blue line indicates a power law decay according to $E(f) \propto f^{-5/3}$.

up to $f \approx 1000\,\text{Hz}$. Frequencies above $f = 40\,\text{kHz}$ are filtered by the data acquisition system.

The investigation of the gust time series and the energy spectral density shows how the recurring gust generated by the chopper can be decomposed into three parts: the mean velocity of the gust, the underlying shape of the gust from the smoothed, phase-averaged signal as recurring large-scale flow structure, and the turbulence within the gust. This triple decomposition is illustrated in figure 5. The gust (figure 5(a)) has a mean gust velocity $\bar{u}$ (figure 5(b)) with an underlying gust shape $\tilde{u}$ (figure 5(c)) with strong turbulent fluctuations u' (figure 5(d)), and $u_G = \bar{u} + \tilde{u} + u'$.

The single elements of gust decomposition can now be used for an extensive analysis.

3.2 Mean gust flow field: $\bar{u}$

In the following, the properties of the mean gust velocity flow field will be investigated by looking at the evolution of $\bar{u}$ across the measured planes. The mean gust velocity is calculated by averaging the individual gust events within a time series and then taking the average over all values. The average standard deviation is determined similarly. For a better comparison between the measurements, the same window with respect to the chopper position is used for all data sets for the respective chopper frequency.

In figure 6, the downstream evolution of the to the inflow velocity normalized average mean gust velocity is presented as interpolated surface plot for both chopper frequencies. For both cases, the mean gust velocity evolves similarly downstream the test section. Close to the inlet, the flow is inhomogeneous along the span-wise direction. The lowest velocities are found at

https://doi.org/10.5194/wes-2019-107
Preprint. Discussion started: 10 January 2020

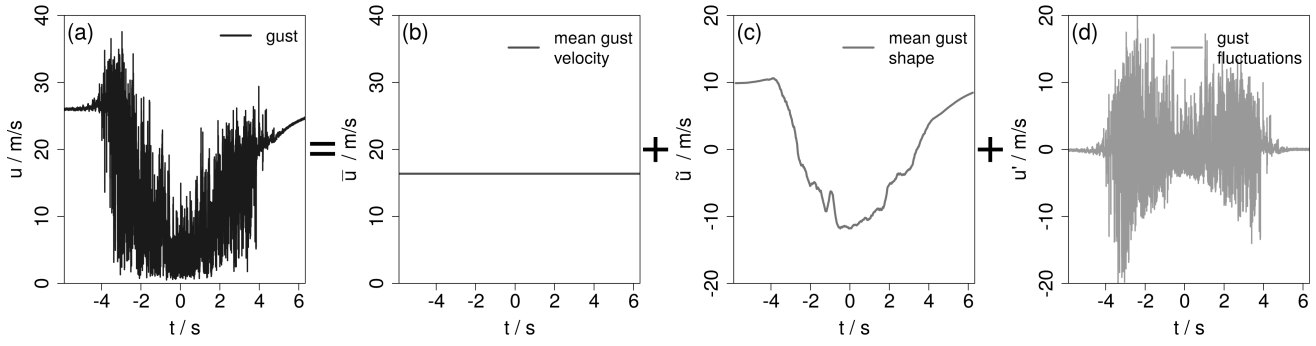

Figure 5. Example for a triple decomposition of the gust $u_G = \bar{u} + \tilde{u} + u'$ (a) into its mean velocity $\bar{u}$ (b), the underlying gust shape $\tilde{u}$ (c), and the fluctuations u' (d).

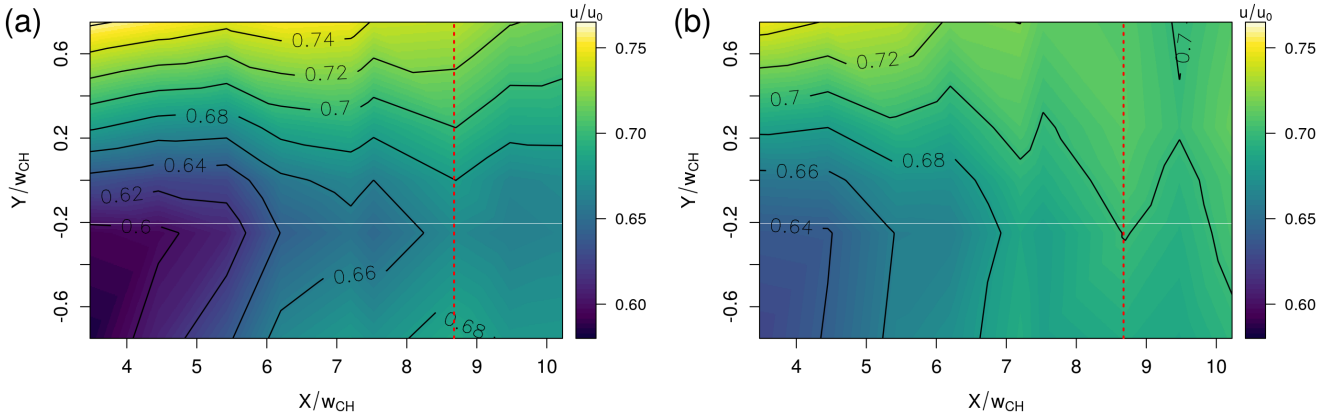

Figure 6. Interpolated surface plot of the downstream evolution of the mean velocity of the gust for (a) $f_{CH1} = 0.04\,\mathrm{Hz}$ and (b) $f_{CH2} = 0.4\,\mathrm{Hz}$. The red dashed line marks the downstream position of the ZY-plane.

the root side of the chopper blade at $X/w_{CH} = 3.475$ and $Y/w_{CH} = -0.75$. At the tip side of the chopper blade at $X/w_{CH} = 3.475$ and $Y/w_{CH} = 0.75$, the velocities are highest. A velocity difference of $0.14u_0$ (or 3.5 m/s) in case of $f_{CH1} = 0.04\,\mathrm{Hz}$ and $0.08u_0$ (or 2.0 m/s) for $f_{CH2} = 0.4\,\mathrm{Hz}$, respectively, is found in span-wise direction at $X/w_{CH} = 3.475$. With increasing downstream position, the flow field becomes more homogeneous in span-wise direction and the average gust velocity reaches approximately 70% of the inflow velocity at the end of the measurement plane. While the flow fields evolve in principle similarly, the velocities are higher and the flow field is less asymmetric in case of the high chopper frequency.

In figure 7, the to the inflow velocity normalized mean gust velocity in the YZ-plane at $X/w_{CH} = 8.675$ is plotted in a similar manner. In case of f_{CH1}, the velocity is lowest in the upper left corner ($Y/w_{CH} = -0.75$, $Z/w_{CH} = 0.75$) where the chopper blade enters the inlet, and highest in the bottom right corner ($Y/w_{CH} = 0.75$, $Z/w_{CH} = -0.75$) where the chopper blade leaves the inlet first. In case of f_{CH2}, the velocity is higher in the right half ($Y > 0$) than in the left half ($Y < 0$).

Next, the average turbulence intensity of the gust is plotted. For this, the average over the standard deviations σ_i of the N

https://doi.org/10.5194/wes-2019-107
Preprint. Discussion started: 10 January 2020

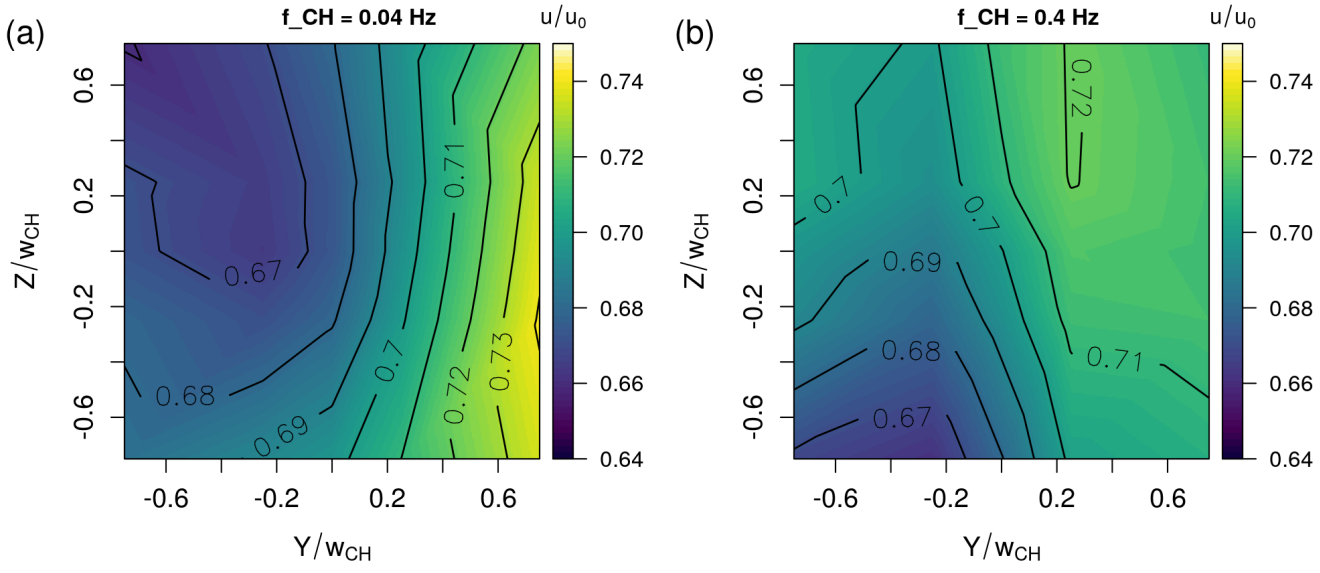

Figure 7. Interpolated surface plot of the mean velocity of the gust in the YZ - plane $8.675 w_{CH}$ downstream the chopper blade for (a) $f_{CH1} = 0.04\,\text{Hz}$ and (b) $f_{CH2} = 0.4\,\text{Hz}$.

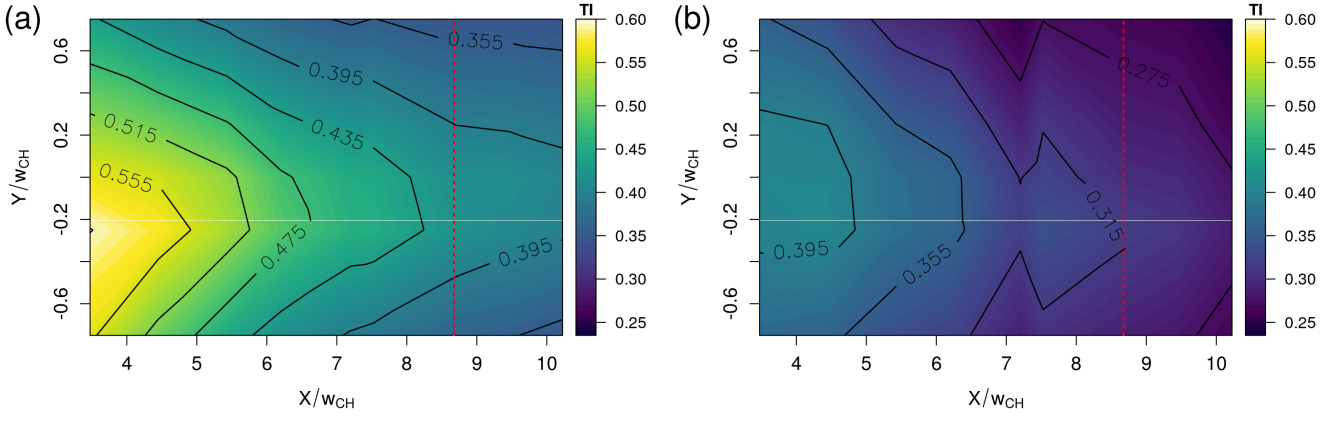

Figure 8. Interpolated surface plot of the turbulence intensity of the gust for (a) $f_{CH1} = 0.04\,\text{Hz}$ and (b) $f_{CH2} = 0.4\,\text{Hz}$. The red dashed line marks the downstream position of the ZY-plane.

gusts within the time series is calculated, $\bar{\sigma}_G = \frac{1}{N}\sum_{i=1}^{N}\sigma_i$, and divided by the average gust velocity, $TI_G = \bar{\sigma}_G/\bar{u}$. The result
130 is presented as interpolated contour plot in figure 8. In case of the lower chopper frequency, the highest turbulence intensities are found closest to the inlet, and the maximum turbulence intensity, $TI_{G,max1} = 60\%$, is measured at $X = 3.475\,w_{CH}$ and $Y/w_{CH} = -0.25$. The flow field is asymmetric but becomes more homogeneous downstream when the turbulence intensity decreases. The lowest value, $TI_{G,min1} = 34\%$, is found at $X/w_{CH} = 10.225$ and $Y/w_{CH} = 0.75$. While the evolution looks

https://doi.org/10.5194/wes-2019-107
Preprint. Discussion started: 10 January 2020

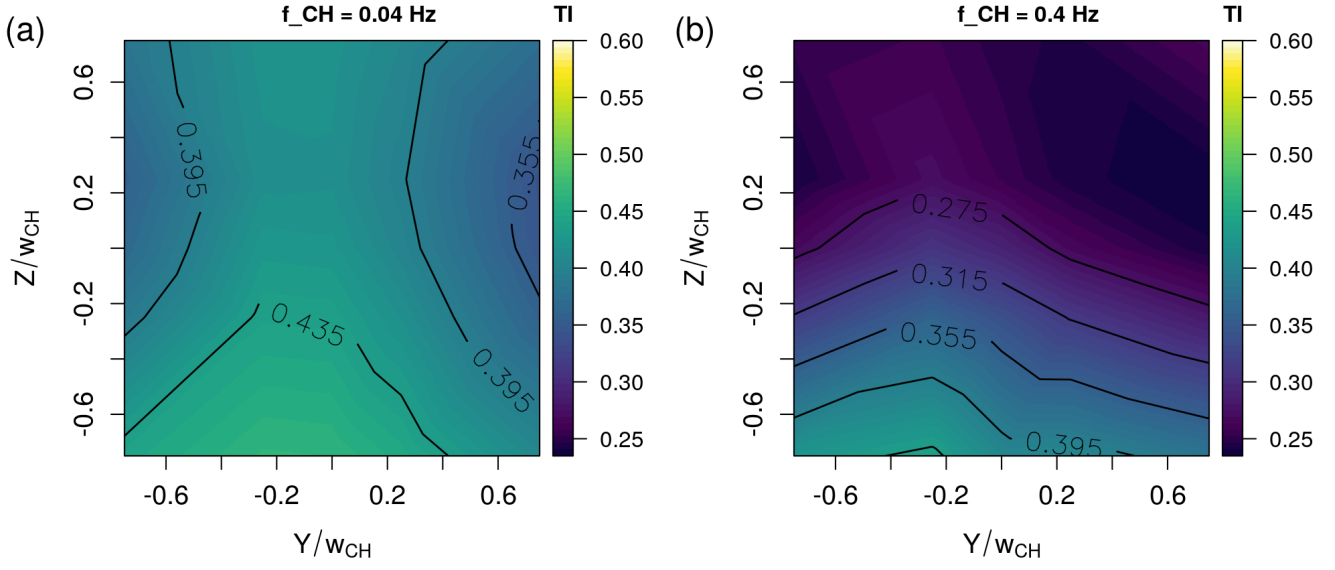

Figure 9. Interpolated surface plot of the turbulence intensity of the gust in the YZ - plane $8.675 w_{CH}$ downstream the chopper blade for (a) $f_{CH1} = 0.04$ Hz and (b) $f_{CH2} = 0.4$ Hz.

as such similarly in case of the high chopper frequency, turbulence intensities are lower, decreasing from $TI_{G,max2} = 41\%$ at $X/w_{CH} = 4.45$ and $Y/w_{CH} = -0.25$ to $TI_{G,min2} = 24\%$ at $X/w_{CH} = 10.225$ and $Y/w_{CH} = 0.75$.

As presented in figure 9, the average gust turbulence intensity does also vary spatially in the YZ-plane ($X/w_{CH} = 8.675$). In case of f_{CH1} (figure 9(a)), the turbulence intensity is lowest at the vertical wind tunnel walls in the upper half of the measurement field and highest in the center in the bottom half. For the high chopper frequency, the average gust turbulence intensity is lowest in the top half of the measurement field and increases in the bottom half.

3.3 Underlying gust shape: $\tilde{u}$

In the following, the underlying gust shape $\tilde{u}$ will be investigated. For this, only the gust segments of each time series are taken into consideration. Exemplarily, in figure 10, all gusts from the respective time series measured at the two chopper frequencies and at the centerline at $X = 5.425\, w_{CH}$ are plotted normalized to the inflow velocity over the with the chopper period $T_{CH} = 1/f_{CH}$ normalized time t. Here $t/T_{CH} = 0$ denotes the horizontal alignment of the chopper blade in the inlet. In black, the smoothed average gust is plotted, and in blue, the blockage of the wind tunnel is added. For both chopper frequencies, the single gusts show strong fluctuations. The maximum velocity fluctuations can reach $1.8u_0$ (or $u \approx 45\, m/s$) ($f_{CH1} = 0.04\, Hz$) or $2.16u_0$ (or $u \approx 54\, m/s$) ($f_{CH2} = 0.4\, Hz$). While the gust generated with a chopper frequency of $f_{CH1} = 0.04\, Hz$ shows a smaller increase of the velocity in the beginning and is mainly characterized by a strong velocity deficit, in case of the faster chopper frequency, $f_{CH2} = 0.4\, Hz$, the increase in the beginning is much stronger and the velocity

https://doi.org/10.5194/wes-2019-107
Preprint. Discussion started: 10 January 2020

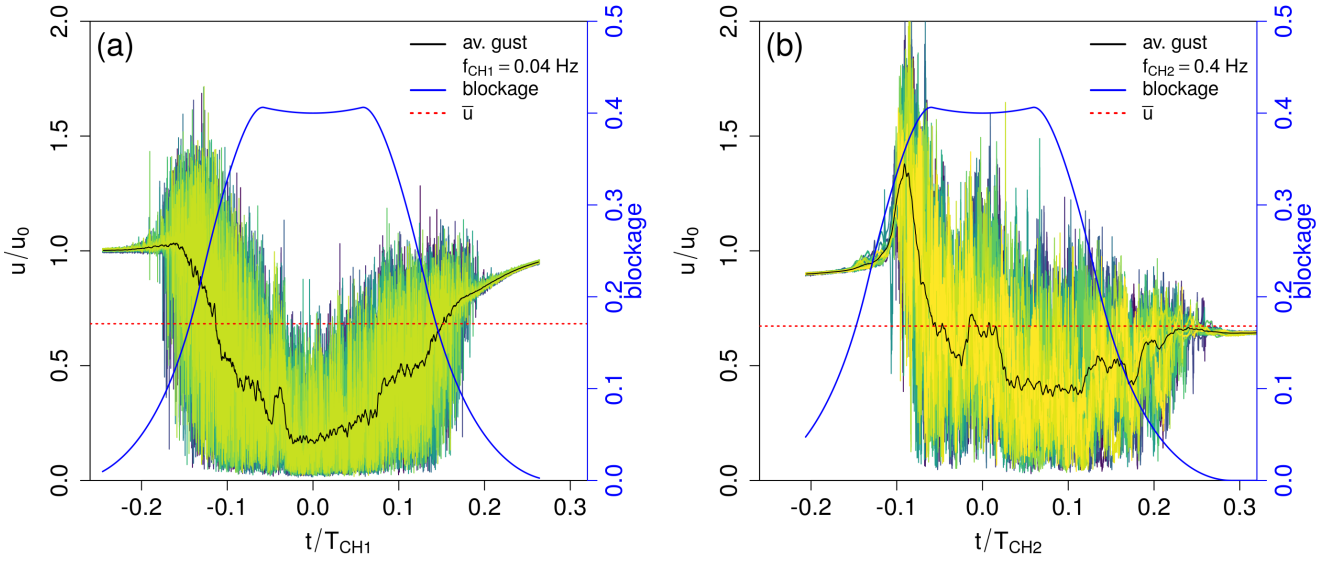

Figure 10. Plot of all gusts captured in the time series measured at the centerline $5.425\,w_{CH}$ downstream the chopper blade for a chopper frequency of (a) $f_{CH1} = 0.04\,\text{Hz}$ and (b) $f_{CH2} = 0.4\,\text{Hz}$. In different colors, the gust events are plotted, in black, the smoothed average gust is marked and in blue, the blockage is added with the corresponding axis on the right side.

deficit afterwards less pronounced.

To increase the understanding of the underlying gust shape $\tilde{u}$ across the width of the wind tunnel, figure 11 shows the to the inflow velocity normalized, smoothed average gust over t/T_{CH} for all span-wise positions and both chopper frequencies at $X/w_{CH} = 3.475$. In case of a low chopper frequency of the chopper (figure 11(a)), the gust shape itself is similar for all span-wise positions. The brief increase in velocity over the inflow velocity is followed by a rapid velocity decrease ($18\,\text{m/s}$ in $2.5\,\text{s}$) and a recovery of the velocity once the chopper blade leaves the inlet. From $Y/w_{CH} = -0.75$ where the chopper blade enters the test section first withe the blade root side, to $Y/w_{CH} = 0.75$ where the chopper blade enters the test section last with the blade tip side, the duration of the gust decreases and its amplitude increases. These observations also hold for the high chopper frequency (figure 11(b)). Moving downstream to the last measurement position at $X/w_{CH} = 10.225$ shows how the gust is transported in stream-wise direction (cf. figure 12). In case of the low chopper frequency (figure 12(a)), the gust disperses, i.e. the duration increases while the amplitude decreases. The minimal velocity within the gust increases while the velocity peak is not present anymore. Also, the underlying gust shape homogenizes and evolves similarly for all span-wise positions. In comparison, the underlying gust shape imprinted onto the flow with a higher chopper frequency (cf. figure 12(b)) preserves the variation in span-wise direction. While the structure disperses as well, the velocity peak at the beginning of the structure is still visible. Due to the downstream transport of the gust, the velocity peaks are found later with respect to the radial chopper blade position that is indicated by the blockage.

With a chopper blade width of w_{CH} as presented in this setup, the gust amplitude is higher than proposed by the ICE-64100-1.

https://doi.org/10.5194/wes-2019-107
Preprint. Discussion started: 10 January 2020

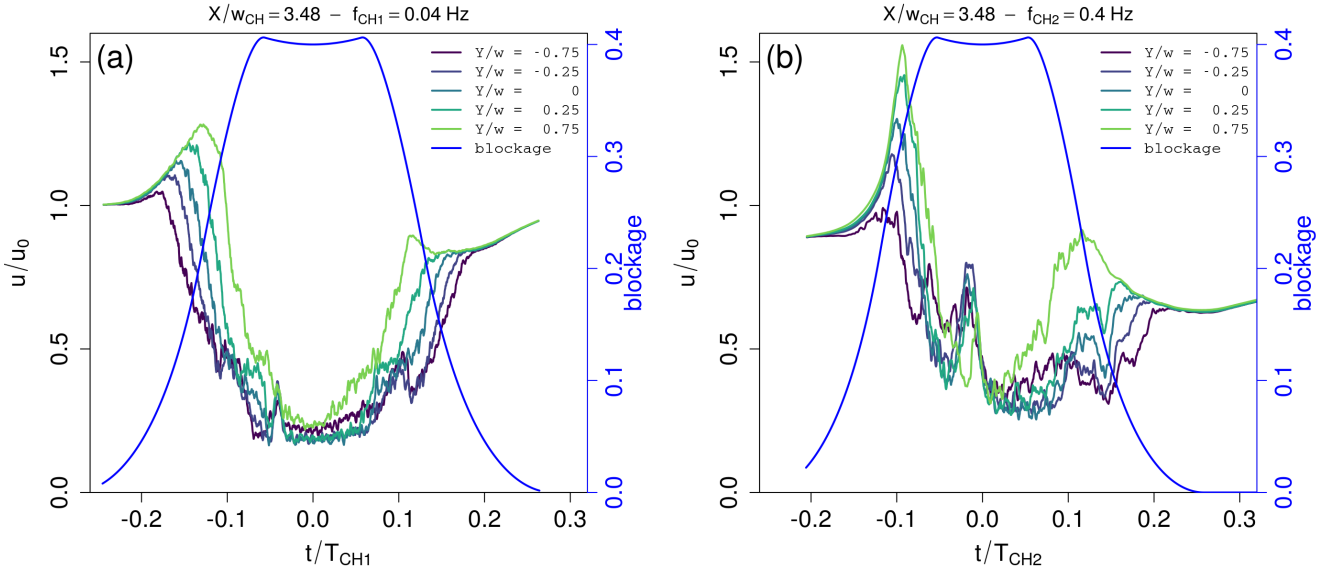

Figure 11. Span-wise evolution of the smoothened average gust at $X/w_{CH} = 3.475$ with respect to the chopper blade position: The gust as measured by the respective sensor is plotted over the normalized time where $t/T_{CH} = 0$ indicates that the chopper blade is aligned horizontally in the inlet, and the blockage is added in blue with the blue axis on the right side. The chopper frequencies are (a) $f_{CH1} = 0.04$Hz and (b) $f_{CH2} = 0.4$ Hz.

The changes in the velocity can be rapid, for example approximately 18 m/s in 2.5 s in case of $f_{CH1} = 0.04\,Hz$ and up to 25 m/s in 0.25 s in case of $f_{CH2} = 0.4\,Hz$.

In order to quantify the duration of the gust and its dispersion, figure 13 shows the to the chopper period normalized downstream evolution of the gust duration $\Delta t/T_{CH}$ for both chopper frequencies and all horizontal measurement positions. The gust duration is calculated by taking the absolute value of the normalized gust fluctuations $u'/\bar{u}$ to find the interval in which the fluctuations frequently exceed a threshold set to be 0.025. For both chopper frequencies, the gust duration increases with increasing distance from the inlet as the gust disperses downstream. Additionally, the gust duration is longer for the inner span-wise measurement positions $Y/w_{CH} = -0.75$ and $Y/w_{CH} = -0.25$ than for the outer span-wise positions ($Y \geq 0$), because the root side of the chopper blade passes by slower than the tip side. Quantitatively, the gust duration scales proportionally to the chopper frequency, which is nicely shown by the similar normalized gust durations for the two chopper frequencies.

3.4 Gust fluctuations: u'

After investigating the mean gust properties and the underlying gust shape, next, some turbulence characteristics of the gust will be discussed by investigating the gust fluctuations u'. Figure 14 shows the energy spectral density of the turbulent fluctuations u' (cf. figure 10 (d)) of all individual gusts captured in the above-discussed time series measured at $X/w_{CH} = 5.425$

https://doi.org/10.5194/wes-2019-107
Preprint. Discussion started: 10 January 2020

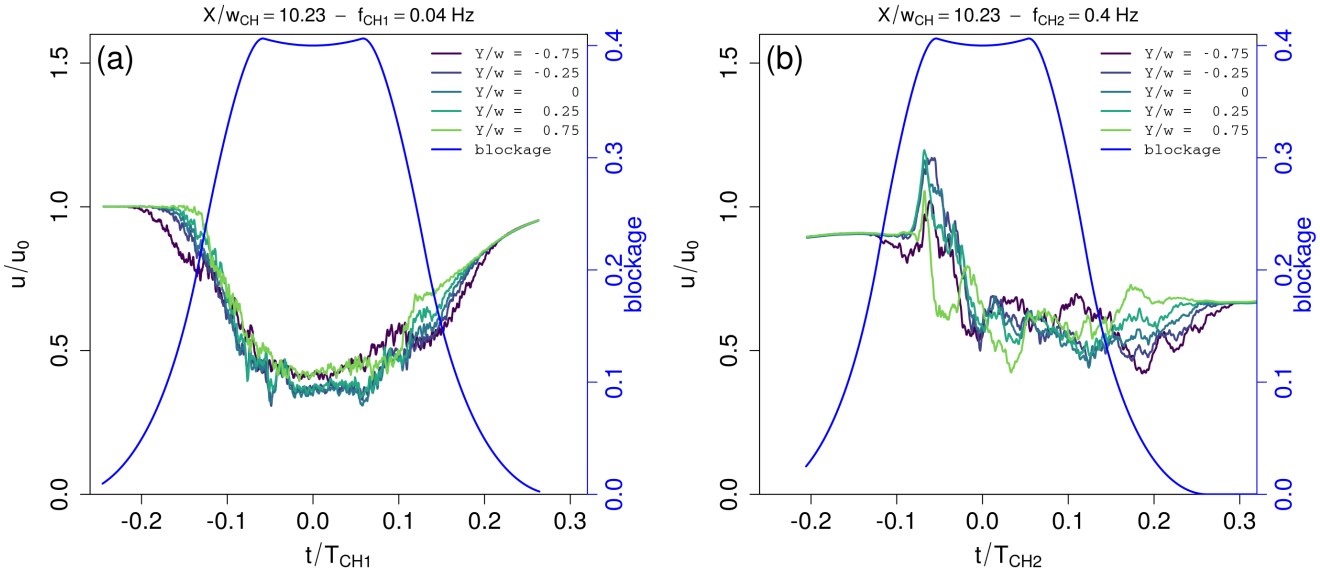

Figure 12. Span-wise evolution of the smoothened average gust at $X/w_{CH} = 10.225$ with respect to the chopper blade position: The gust as measured by the respective sensor is plotted over the normalized time where $t/T_{CH} = 0$ indicates that the chopper blade is aligned horizontally in the inlet, and the blockage is added in blue with the blue axis on the right side. The chopper frequencies are (a) $f_{CH1} = 0.04$Hz and (b) $f_{CH2} = 0.4$ Hz.

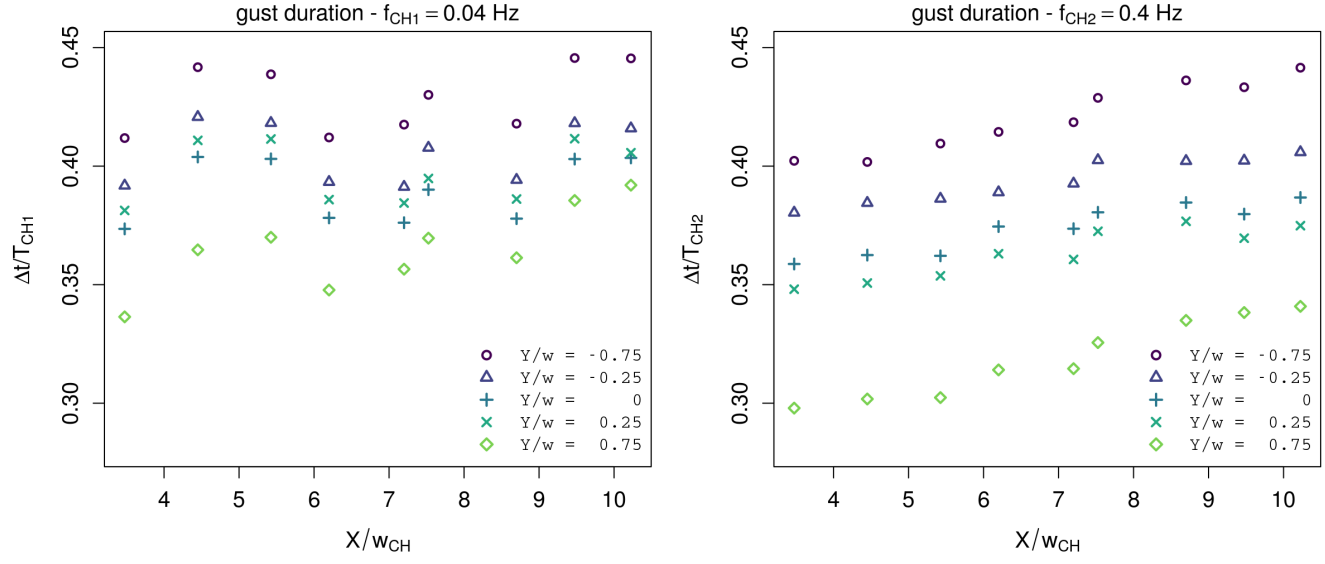

Figure 13. Average normalized duration $\Delta t/T_{CH}$ of the gusts at the respective span-wise and downstream positions for (a) $f_{CH1} = 0.04$Hz and (b) $f_{CH2} = 0.4$ Hz.

https://doi.org/10.5194/wes-2019-107
Preprint. Discussion started: 10 January 2020

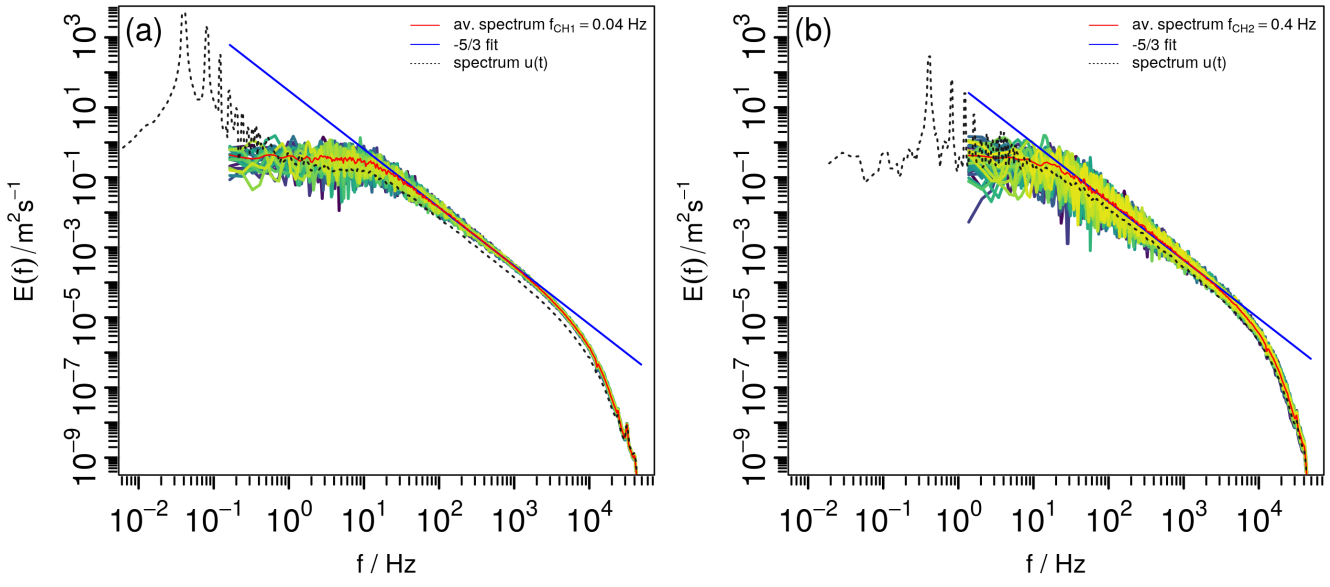

Figure 14. Energy spectral density of all gusts (blue-green-yellow color map) with the average spectrum plotted in red and a decay according to $E(f) \propto f^{-5/3}$ plotted in blue. The downstream position is $X = 5.425\, w_{CH}$, the measurement was carried out at the centerline and the chopper frequency is (a) $f_{CH1} = 0.04$ Hz and (b) $f_{CH2} = 0.4$ Hz.

for the respective chopper frequencies. In addition, the average over all spectra is plotted in red, and the decay according to $E(f) \propto f^{-5/3}$ in the inertial sub-range is indicated in blue. The plots show that the turbulence within the gust has approx-
185 imately the same energy spectrum for all gusts. The inertial sub-range follows a decay according to $E(f) \propto f^{-5/3}$ in the frequency range between $20\,\text{Hz} \leq f \leq 2000\,\text{Hz}$ ($f_{CH1} = 0.04\,\text{Hz}$) and $20\,\text{Hz} \leq f \leq 5000\,\text{Hz}$ ($f_{CH2} = 0.4\,\text{Hz}$), respectively. To further characterize the gust turbulence, the one-dimensional energy spectrum is as suggested by Hinze (1975) used to calculate the integral length scale $L = \lim_{f \to \infty} \left(\frac{E(f) \cdot \overline{u}}{4\sigma^2} \right)$ of the turbulence. The results are shown for both chopper frequencies as interpolated contour plots in figure 15. While in case of the lower chopper frequency $f_{CH1} = 0.04\,\text{Hz}$, higher values of L
190 are present, the evolution of L across the measurement plane behaves in principle similarly: L increases both in span-wise direction from $Y/w_{CH} = -0.75$ to $Y/w_{CH} = 0.75$ and downstream from $X/w_{CH} = 3.475$ to $X/w_{CH} = 10.225$. With respect to the average integral length $\bar{L}$ over the whole flow field, the gradient in span-wise direction is approximately 20% in case of f_{CH1} and between 20% ($X/w_{CH} = 3.475$) and 0.6% ($X/w_{CH} = 10.225$) in case of f_{CH2}. The downstream gradients are 63% and 40%, respectively, which indicates that the change in streamwise direction is more significant. The smallest values
195 are found at $X/w_{CH} = 3.475$ and $Y/w_{CH} = -0.75$ with $L = 0.25\, w_{CH}$ in case of $f_{CH1} = 0.04\,\text{Hz}$ and $L = 0.245\, w_{CH}$ in case of $f_{CH2} = 0.4\,\text{Hz}$, respectively. As the turbulence evolves downstream, L increases and the highest values are found at the opposite corner of the flow field at $X/w_{CH} = 10.225$ and $Y/w_{CH} = 0.25$ with $L = 0.73\, w_{CH}$ in case of $f_{CH1} = 0.04\,\text{Hz}$

https://doi.org/10.5194/wes-2019-107
Preprint. Discussion started: 10 January 2020

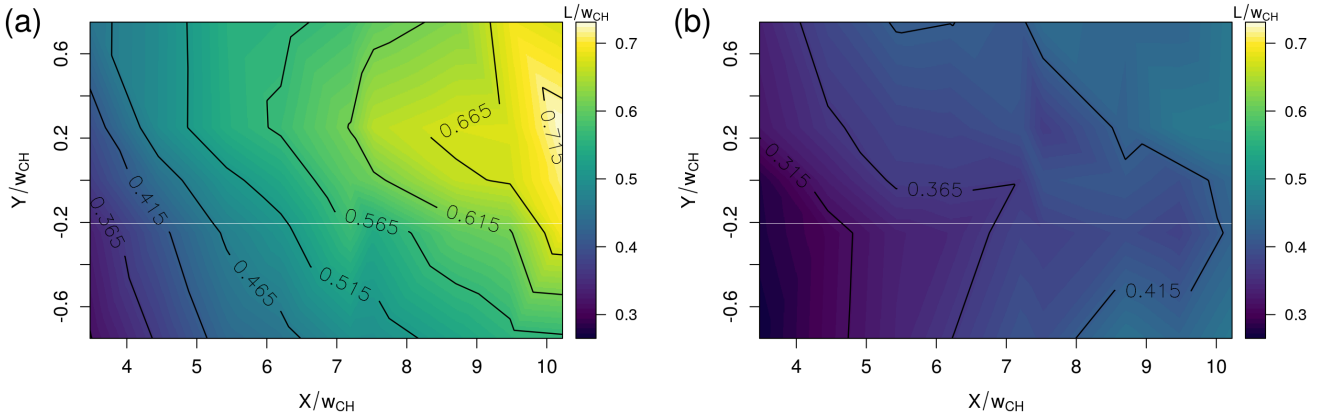

Figure 15. Interpolated surface plot of the integral length scale of the gust fluctuations for (a) $f_{CH1} = 0.04\,\text{Hz}$ and (b) $f_{CH2} = 0.4\,\text{Hz}$.

and $L = 0.46\,w_{CH}$ in case of $f_{CH2} = 0.4\,\text{Hz}$.

4 Discussion

In the previous section, it was presented how the gust generated by the chopper can be decomposed into into its mean velocity $\bar{u}$, the underlying gust shape $\tilde{u}$, and the fluctuations u'. By means of the single components, the characteristics and the evolution of the gust have been presented. It was shown how the gust has a duration Δt that scales proportionally to the chopper frequency. From the gust fluctuations, an integral length scale could be calculated by means of the energy spectral density. This shows how the gust can be characterized by two scales, its duration as an 'outer' scale and the integral length of the fluctuations as an 'inner' scale. Additionally, a comparison between the spectrum of the fluctuating part and the spectrum of the respective whole time series (cf. figure 4), indicated in a dashed line, reveals that both spectra have a similar behavior in the high frequency range. The small offset between the spectra can be explained by the normalization to the respective variance. This leads to the interpretation that the triple decomposition also holds in the spectral domain where the periodically recurring underlying gust shape is mirrored in the high-energetic, low-frequent part of the spectrum, and the gust fluctuations are mirrored in the high-frequent part of the spectrum that decays as expected from turbulence theory according to $E(f) \propto f^{-5/3}$. To verify this interpretation, figure 16 shows how the spectrum of the time series $E_G(f)$, (a), can be decomposed into a high-energetic low-frequent part $\tilde{E}(f)$, (b), and a high-frequent decaying part $E'(f)$, (c), by calculating the spectra of the signal filtered by a second order butterworth filter (see e.g.Proakis and Manolakis (1992)) and the gust fluctuations, respectively.

https://doi.org/10.5194/wes-2019-107
Preprint. Discussion started: 10 January 2020

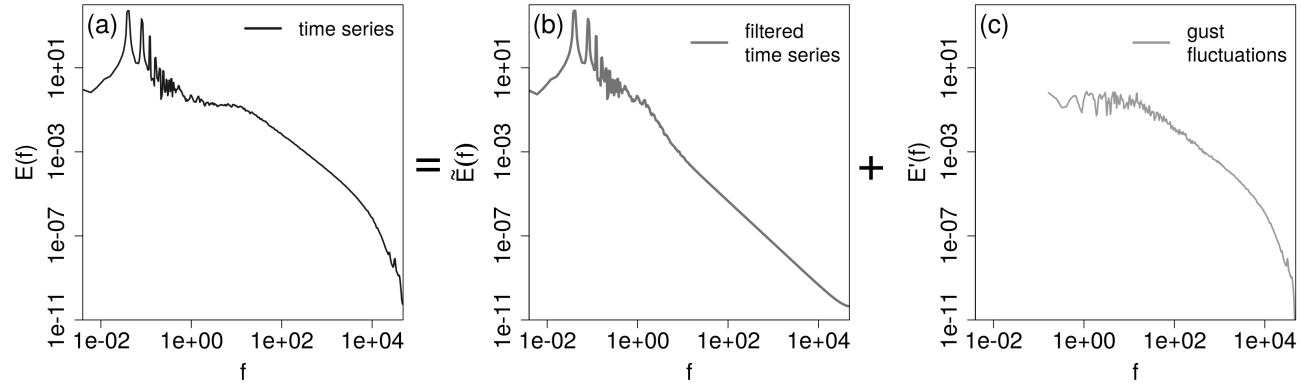

Figure 16. Example for a spectral decomposition of the gust $E_G(f) = \tilde{E}(f) + E'(f)$ (a) into its periodic, high-energetic part $\tilde{E}(f)$ (b) and the spectrum of the fluctuations $E'(f)$ (c).

5 Conclusions and Outlook

A new system for the generation of strong, sudden gusts in a wind tunnel, the chopper, has been presented. The gust structure generated by the chopper has been investigated for a fixed inflow velocity and two different chopper frequencies. First, the periodic flow variation that is generated each time the chopper blade crosses the inlet was discussed by means of the time series and its energy spectrum. To gain a better understanding of the gust structure itself, in the next step, the gust events were brought into focus. It was shown how the gust has an underlying shape with superimposed fluctuations, so that each gust can be decomposed into a mean gust velocity, the underlying gust shape and the high-frequent fluctuations. For the further analysis, this triple decomposition was used to discuss the downstream evolution of the underlying gust shape that disperses downstream while the average gust velocity increases and the turbulence intensity decreases downstream. The gust duration is proportional to the chopper frequency. The mean gust amplitude is larger than the one proposed in the IEC-64100-1 for all measurements. In addition, the velocity can change rapidly. The fluctuations were analyzed by means of the energy spectrum that shows a classical turbulence decay with an inertial sub-range that decays according to $E(f) \propto f^{-5/3}$ and an integral length scale that increases downstream as the turbulence evolves and is in the order of magnitude of half the chopper blade width. It was confirmed that the gust can be characterized by an outer scale, namely its duration, and an inner scale, namely the integral length, by introducing the decomposition of the energy spectral density into a low-frequent, high-energetic part and a high-frequent decaying part.

Overall, a new system was presented that is capable of generating large velocity fluctuations while also inducing turbulence. By means of the downstream position and the chopper frequency, experiments can be executed in different regions of the flow field with different characteristics and different complexity that increases towards the inlet.

Next steps will be the investigation of the other flow components with 2D and 3D measurement techniques,the variation of the chopper blade width to generate gusts with different amplitudes and the installation of a regular square grid upstream the chopper to add background turbulence.

https://doi.org/10.5194/wes-2019-107
Preprint. Discussion started: 10 January 2020

eawe european academy of wind energy
Open Access WIND ENERGY SCIENCE DISCUSSIONS

Author contributions. System design, C. B.; Data acquistion, I. N.; Formal analysis, I. N.; Funding acquisition, C. B.; Investigation, I. N.; Methodology, I. N.; Project administration, C. B.; Resources, C. B.; Writing - original draft, I. N.; Writing - review & editing, C. B.

Competing interests. The authors declare no conflict of interest

Acknowledgements. This project is funded by WEAMec, Pays de la Loire, Ecole Centrale Nantes and Nantes Metropole.

https://doi.org/10.5194/wes-2019-107
Preprint. Discussion started: 10 January 2020

eawe european academy of wind energy
Open Access WIND ENERGY SCIENCE DISCUSSIONS

References

Frandsen, S.: Turbulence and turbulence generated structural loading in wind turbine clusters, Phd thesis, DTU - Risø National Laboratory, 2007.

Hideharu, M.: Realization of a large-scale turbulence field in a small wind tunnel, Fluid Dynamics Research, 8, 53–64, https://doi.org/10.1016/0169-5983(91)90030-m, https://doi.org/10.1016%2F0169-5983%2891%2990030-m, 1991.

Hinze, J.: Turbulence, McGraw-Hill classic textbook reissue series, McGraw-Hill, 1975.

Hultmark, M. and Smits, A. J.: Temperature corrections for constant temperature and constant current hot-wire anemometers, Measurement Science and Technology, 21, 105 404, https://doi.org/10.1088/0957-0233/21/10/105404, https://doi.org/10.1088%2F0957-0233%2F21%2F10%2F105404, 2010.

IEC-61400-1-4: IEC 61400-1-4: Wind energy generation systems - Part 1: Design requirements, Report, International Electrotechnical Commission, 2019.

Lee, S., Churchfield, M., Moriarty, P., Jonkman, J., and Michalakes, J.: Turbulence Impacts on Wind Turbine Fatigue Loadings, 50th AIAA Aerospace Sciences Meeting including the New Horizons Forum and Aerospace Exposition, Aerospace Sciences Meetings, pp. 175–191, https://www.nrel.gov/docs/fy12osti/53567.pdf, 2012.

Petrović, V., Berger, F., Neuhaus, L., Hölling, M., and Kühn, M.: Wind tunnel setup for experimental validation of wind turbine control concepts under tailor-made reproducible wind conditions, J. Phys.: Conf. Ser., 1222, https://doi.org/doi:10.1088/1742-6596/1222/1/012013, 2019.

Proakis, J. G. and Manolakis, D. G.: Digital Signal Processing (2nd Ed.): Principles, Algorithms, and Applications, Macmillan Publishing Co., Inc., Indianapolis, IN, USA, 1992.

Tang, D. M., Paul, G. A., and Dowell, E. H.: Experiments and Analysis for a Gust Generator in a Wind Tunnel, J Aircraft, 1996.

Traphan, D., Wester, T. T. B., Peinke, J., and Gülker, G.: On the aerodynamic behavior of an airfoil under tailored turbulent inflow conditions, Proceedings of the 5th International Conference on Experimental Fluid Mechanics ICEFM 2018 Munich, https://www.researchgate.net/publication/326300998_On_the_aerodynamic_behavior_of_an_airfoil_under_tailored_turbulent_inflow_conditions, 2018.

Wei, N. J., Kissing, J., Wester, T. T. B., Wegt, S., Schiffmann, K., Jakirlic, S., Hölling, M., Peinke, J., and Tropea, C.: Insights into the periodic gust response of airfoils, Journal of Fluid Mechanics, 876, 237–263, https://doi.org/10.1017/jfm.2019.537, 2019a.

Wei, N. J., Kissing, J., and Tropea, C.: Generation of periodic gusts with a pitching and plunging airfoil, Experiments in Fluids, 60, 166, https://doi.org/10.1007/s00348-019-2815-1, 2019b.

Wester, T. T. B., Kampers, G., Gülker, G., Peinke, J., Cordes, U., Tropea, C., and Hölling, M.: High speed PIV measurements of an adaptive camber airfoil under highly gusty inflow conditions, J. Phys.: Conf. Ser., 1037, https://doi.org/doi:10.1088/1742-6596/1037/7/072007, 2018.